Environ Fluid Mech (2017) 17:27–46
DOI 10.1007/s10652-015-9442-z

ORIGINAL ARTICLE

Self-aeration in the rapidly- and gradually-varying flow regions of steep smooth and stepped spillways

Gangfu Zhang[1] · **Hubert Chanson**[1]

Received: 9 August 2015 / Accepted: 15 December 2015 / Published online: 24 December 2015
© Springer Science+Business Media Dordrecht 2015

Abstract In high-velocity chute flows, free-surface aeration is often observed. The phenomenon is called self-aeration or white waters. When the turbulent shear stresses next to the free-surface are large enough, air bubbles are entrained throughout the entire air–water column. A rapidly-varied flow region is observed immediately downstream of the inception point of free-surface aeration. An analytical solution of the air diffusion equation is proposed and the results compare well with new experimental data. Both experiments and theory indicate that the flow bulking spans over approximately 3–4 step cavities downstream of the inception point of free-surface aeration on a stepped chute. Further downstream the void fraction distributions follow closely earlier solutions of the air diffusion equation. The application of the diffusion equation solution to prototype and laboratory data shows air bubble diffusivities typically larger than the momentum transfer coefficient. The result highlights however a marked decrease in the ratio of air bubble diffusivity to eddy viscosity with increasing Reynolds number. The finding might indicate some limitation of laboratory investigations of air bubble diffusion process in self-aerated flows and of their extrapolation to full-scale prototype applications.

Keywords Air entrainment · Self-aeration · Smooth chutes · Stepped spillways · Rapidly-varied flow

1 Introduction

In high-velocity open channel flows, free-surface aeration, also called self-aeration, is commonly observed [8, 20, 37, 40]. Figure 1 illustrates typical examples of self-aeration in prototype spillways. The process of free-surface aeration in chutes and spillways was

✉ Hubert Chanson
h.chanson@uq.edu.au;
http://www.uq.edu.au/~e2hchans/

[1] The University of Queensland, School of Civil Engineering, Brisbane, QLD 4072, Australia


A
B
C

◀**Fig. 1** Free-surface aeration on smooth and stepped prototype spillways, including details of the rapidly-varied flow region immediately downstream of the inception point of free-surface aeration. **a** Somerset dam (Australia) on 28 January 2013—Gates fully-opened: Q ~ 450 m^3/s (q ~ 8 m^2/s), Re 3 × 10^7, smooth chute, shutter speed: 1/400 s (*left*) and 1/3,200 s (*right*). **b** Hinze dam (Autralia) on 29 January 2013—Q 203 m^3/s, d_c/h ~ 2.53, Re ~ 6.6 × 10^7, stepped chute (θ = 51.3°, h = 1.2 m)—*left* general view from downstream (shutter speed: 1/4000 s); *right* view from upstream looking at the large-scale free-surface structures (boils) next to the inception point of free-surface (shutter speed: 1/1000 s). **c** Paradise dam (Australia) on 5 March 2013—Q 2300 m^3/s, $d_c/h = 2.86$, Re 2.7 × 10^7, stepped chute (θ = 57.4°, h = 0.62 m)—*left* general view from right bank (shutter speed: 1/1250 s); *right* details of free-surface structures next to the inception point of free-surface (shutter speed: 1/1250 s)

originally investigated because of the induced air–water flow bulking, the drag reduction induced by bubbles next to the invert, the reduction in cavitation damage and the air–water mass transfer [22, 36, 47]. On both smooth and stepped chutes, a turbulent boundary layer develops at the upstream end. When the boundary layer outer edge is close to the free-surface, the turbulent shear stress next to the free-surface is large enough to overcome both the surface tension and buoyancy effects and free-surface aeration occurs [15, 21]. This location is called the inception point of free-surface aeration [12, 27, 48]. It is clearly seen in prototype chutes (Fig. 1). On smooth spillways, surface waves are seen immediately upstream of the inception, as well as longitudinal streaks [2, 30]. On stepped spillways, prototype and laboratory observations showed the presence of large surface scars directly upstream of the inception point and some surface flapping [9, 16] (Fig. 1b). The flow measurements about the inception point showed intense free-surface aeration in this very rapidly-varied flow region: "*at the point of inception […] the mean concentration is approximately 0.2*" [32]. The finding was confirmed experimentally for a range of slopes [3, 6, 18, 33, 39].

After a brief bibliography, the paper presents a new analysis of the air bubble diffusion in the rapidly-varied flow region immediately downstream of the inception point of free-surface aeration. An analytical solution is compared with existing solutions of the diffusion equation in uniform equilibrium flow. The results are compared with new experimental data obtained in the rapidly-varied flow region and in the gradually-varied flow downstream. The results are also presented in term of the air bubble diffusion coefficient. The outcomes are discussed in terms of the ratio of turbulent diffusivity to momentum transfer coefficient.

1.1 Bibliography

Since the first successful air–water flow measurements of Ehrenberger [20], a few early models of air bubble diffusion were derived from sediment-laden flow studies assuming uniform equilibrium: e.g., the model of Straub and Anderson [38] (Table 1). Straub and Anderson proposed a two-layer model, with an inner/lower region consisting of air bubbles distributed through water by turbulent transport fluctuations and an outer/upper flow region with a heterogeneous mixture of water droplets ejected from the flowing stream [26, 38]. The model was extended numerically, taking into account a non-uniform velocity profile [28]. In contrast, Rao and Gangadharaiah [35] and Wood [45] developed the conservation equation for the air–water mixture density assuming a homogeneous air–water mixture between 0 and Y_{90}, where Y_{90} is the distance normal to the invert where the void fraction C = 0.90. Measured void fraction and velocity distributions indeed showed that the air–water flow motion behaves as a homogeneous gas–liquid mixture between 0 and Y_{90} [8,

Table 1 Air diffusion model solutions for self-aerated smooth and stepped chute (skimming) flows

Reference	Void fraction distribution	Discussion
[38]	$C = C_T \times \left(\frac{y}{d_T - y}\right)^{z'}$ $\frac{1-C}{1-C_T} = \frac{2}{h' \times \sqrt{\pi}} \times \int_{y-d_T}^{+\infty} \exp\left(-\left(\frac{u}{h'}\right)^2\right) \times du$	Uniform equilibrium flow—lower flow region ($y < d_T$) Uniform equilibrium flow—upper flow region ($y > d_T$)
[35]	$\frac{1-C}{1-C_D} = \frac{1}{2} \times \left(1 - \text{erf}\left(\frac{y}{b \times E \times (x - L_i)}\right)\right)$	Gradually-varied flow ($0 < y < Y_{90}$)
[45]	$C = \frac{B'}{B' + \exp\left(-G' \times \cos\theta \times \left(\frac{y}{Y_{90}}\right)^2\right)}$	Uniform equilibrium and gradually-varied flows ($0 < y < Y_{90}$)
[13]	$C = 1 - \tanh^2\left(K' - \frac{y/Y_{90}}{2 \times D'}\right)$	Uniform equilibrium and gradually-varied flows ($0 < y < Y_{90}$) $K' = 0.32745 + 0.5/D'$ $D' = 0.75699 \times C_{mean}^{1.0104}$
[18]	$C = 1 - \tanh^2\left(K'' - \frac{y/Y_{90}}{2 \times D_o} + \frac{(y/Y_{90} - 1/3)^3}{3 \times D_o}\right)$	Uniform equilibrium and gradually-varied flows ($0 < y < Y_{90}$) $D' = \frac{D_o}{1 - 2 \times \left(\frac{y}{Y_{90}} - \frac{1}{3}\right)^2}$ $K'' = 0.32745 + 0.40123/D_o$ $D_o = -0.2767 \times \text{Ln}(1.0434 - 1.312 \times C_{mean})$
Present study	$C = 0.5 \times \text{erfc}\left(\frac{Y_{50} - y}{2 \times \sqrt{\frac{D_t \times (x - L_i)}{V}}}\right)$	Rapidly-varied flow immediately downstream of inception point of free-surface aeration ($0 < y < +\infty$)

11, 14, 46, 47]. The model of Rao and Gangadharaiah [35] was proposed for gradually-varied flows, but required the determination of a significant number of semi-empirical parameters. Although developed for the equilibrium region, Wood's [45] model provided a simpler expression and an excellent fit of smooth invert data in both gradually-varied and equilibrium flow regions. But the model used empirical constants derived from the concept of "*diffusivity of the average density*" and the need to estimate a "*fall velocity of water*".

Two newer models were developed based upon analytical solutions of the diffusion equation for air bubbles in the equilibrium region [13, 18] (Table 1). Chanson [13] assumed a constant dimensionless diffusivity D' across the water column, with D' being solely a function of the depth-averaged void fraction C_{mean}. Chanson and Toombes [18] proposed a non-constant diffusivity D' across the water column (Table 1, column 3). Both models compared well with experimental data in the equilibrium and gradually-flow regions, although Chanson's [13] model tended to fit better smooth chute flow data, and the model of Chanson and Toombes [18] skimming flow data on stepped chutes. This is illustrated in Fig. 2, showing both smooth and stepped chute data compared to these two solutions.

2 Basic considerations

Considering a two-dimensional flow as illustrated in Fig. 3 and assuming the advective transport terms to be small, the equation of conservation of mass for air may be expressed as [14]:

$$\frac{\partial}{\partial t}C = \text{div}\left(D_t \times \overrightarrow{\text{grad}}C - C \times \vec{u_r}\right) \quad (1)$$

where C is the time-averaged void fraction, t is the time, D_t is the turbulent diffusivity and u_r is the bubble rise velocity.

Considering the rapidly-varied flow region immediately downstream of the inception point, the upstream boundary conditions at the inception point ($x = L_i$) are: $C = 1$ for $y > d_i$ and $C = 0$ for $y < d_i$, where x is the longitudinal coordinate with $x = 0$ at the spillway crest, L_i is the longitudinal distance where the inception of free-surface aeration takes place, y is the distance normal to the chute invert, d_i is the flow depth at inception (Fig. 3). For $x > L_i$, the time of travel between L_i and any streamwise position x is: $t = (x - L_i)/V_a$, where V_a is the mean flow velocity, averaged over the distance between x and L_i. In first approximation, Eq. (1) may be reduced to a one-dimensional diffusion equation in terms of void fraction governed by Fick's second law:

$$\frac{\partial C}{\partial t} = D_t \times \frac{\partial^2 C}{\partial y^2} \quad (2)$$

assuming that $\partial C/\partial x \ll \partial C/\partial y$ and neglecting buoyancy effects. This scenario is analogous to that of an inter-diffusion between two semi-infinite masses as long as the diffusion layer remains thin compared to the flow depth (Fig. 3). If the diffusion layer extends to the invert (or pseudo-bottom formed by the step edges), a complete solution may be obtained using the method of images, although preliminary calculations showed that the invert had virtually no effect on the accuracy of solution under current experimental conditions (see below). The boundary conditions for Eq. (2) are: $C(y = +\infty, t > 0) = 1$ and $C(y = -\infty, t > 0) = 0$. The solution of Eq. (2) is:

A

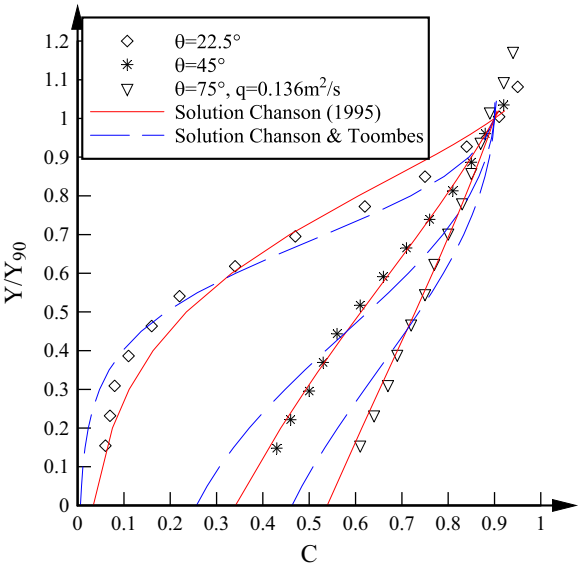

B

Slope	q (m^2/s)	Re	Step	C_{mean}	Reference
8.9	0.099	3.9×10^5	21	0.33	Felder and Chanson (2013)
26.6	0.090	3.6×10^5	13	0.34	Bung (2009)
50	0.35	1.4×10^6	45	0.59	Boes (2000)

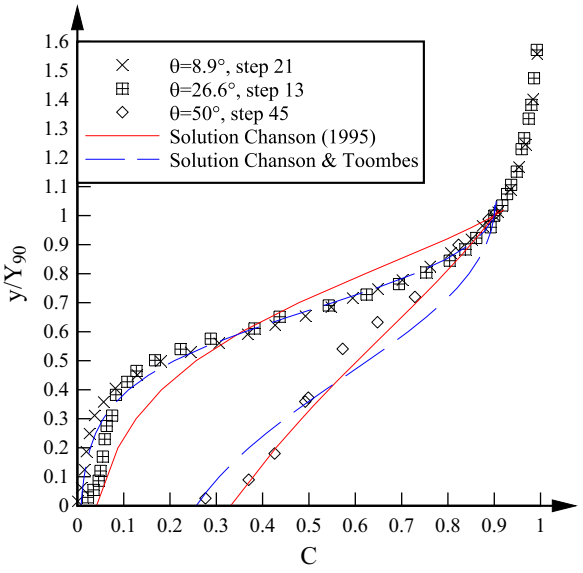

Fig. 2 Void fraction distributions in self-aerated chute flows. **a** Uniform equilibrium flows in a smooth chute for θ = 22.5°, 45° and 75°—Data: Straub and Anderson [38], q = 0.136 m^2/s, Re = 5.4 × 10^5—comparison with analytical solutions by Chanson [13] (*red*) and Chanson and Toombes [18] (*blue*). **b** Gradually-varied and uniform equilibrium skimming flows on stepped chutes—comparison with analytical solutions by Chanson [13] (*red*) and Chanson and Toombes [18] (*blue*) for θ = 26.6° and 50°

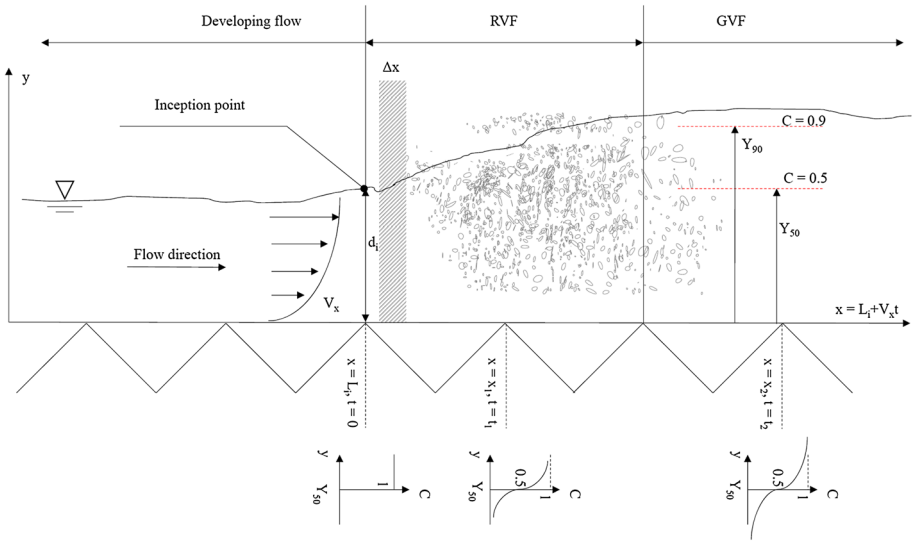

Fig. 3 Longitudinal development of air entrainment in a stepped chute flow

$$C = \frac{1}{2} \times \text{erfc}\left(\frac{1}{2} \times \frac{Y_{50} - y}{\sqrt{\frac{D_a \times (x - L_i)}{V_a}}}\right) \tag{3}$$

where erfc is the complementary error function, Y_{50} is the elevation where $C = 0.50$, and D_a is an apparent time-averaged diffusivity:

$$D_a = \frac{1}{T} \times \int_0^T D_t \times dt \tag{4}$$

with $D_a = D_t$ in uniform flow with homogeneous turbulence and the integration time T being larger than the characteristic time scales of turbulent fluctuations. This new solution (Eq. 3) is valid for the rapidly-varying flow immediately downstream of the inception and presents some similarity with that obtained for a water jet discharging into atmosphere [4, 10, 14]. Equation (3) is compared to experimental data in Fig. 4a, with the diffusivity being selected based upon a best fit and $t = 0.01$ s at the location of inception. A good agreement was observed over the first two step edges downstream of the inception point of free-surface aeration which corresponded to the rapidly-varied flow region. In the gradually-varied flow region further downstream, Eq. (3) tended to underpredict the void fraction next to the invert (step edge 12, Fig. 4a) because the buoyancy effects were unaccounted for, although the agreement with experimental data remained good for $0.2 < C < 0.9$. The analytical solutions of Chanson [13] and Chanson and Toombes [18] might be more appropriate in this case.

In the gradually-varied and uniform equilibrium air–water flow regions, Eq. (1) may be simplified into [13, 14]:

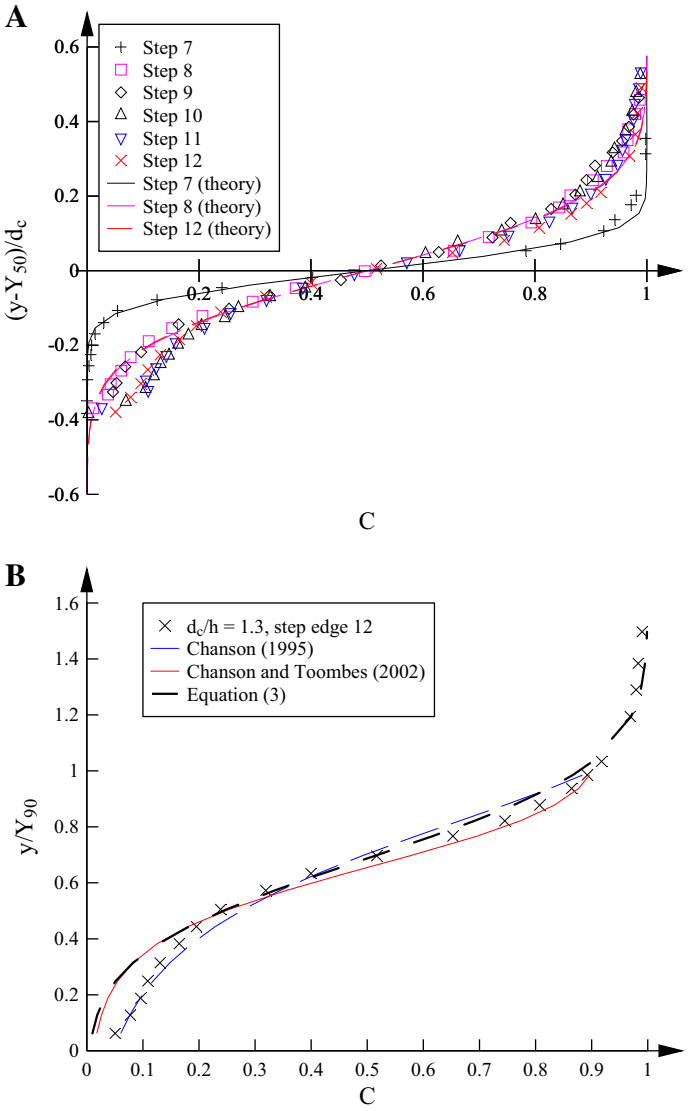

Fig. 4 Void fraction distributions in skimming flows on a stepped spillway ($\theta = 45°$, $h = 0.1$ m, $d_c/h = 1.3$, inception point at step edge 7). **a** Void fraction distributions in the rapidly-varied flow region—comparison between Eq. (3) and data. **b** Comparison between experimental data at step edge 12 and various void fraction models [13, 18], Present study (Eq. 3)

$$0 = \frac{\partial}{\partial y}\left(D_t \times \frac{\partial C}{\partial y}\right) - \cos\theta \times \frac{\partial}{\partial y}\left(C \times \sqrt{1 - C} \times (u_r)_o\right) \quad (5)$$

where θ is the spillway invert slope and $(u_r)_o$ is the bubble rise velocity in clear-water with a hydrostatic pressure gradient. Analytical solutions were developed for $y < Y_{90}$ where Y_{50} is the elevation where $C = 0.90$ and they are reported in Table 1. Three diffusion

models were compared to experimental data recorded at the downstream end of a steep stepped chute in Fig. 4b. The model of Chanson [13] provided the best fit in the lower part of the flow, while both Eq. (3) and Chanson and Toombes' [18] solution underpredicted the void fraction in that region. Note that the present model is applicable for $y < +\infty$.

3 Experimental observations

New experiments were performed in a 5 m long 0.985 m wide test section, consisting of a 1.2 m high broad crested weir followed by 12 steps, 0.10 m long and 0.10 m high each (Fig. 5). Water was fed from a large intake basin though a 2.8 m long sidewall convergent with a contraction ration of 5.08:1 ensuring a smooth and waveless inflow. Air–water flow properties were measured with a double-tip phase detection probe. Each needle sensor had

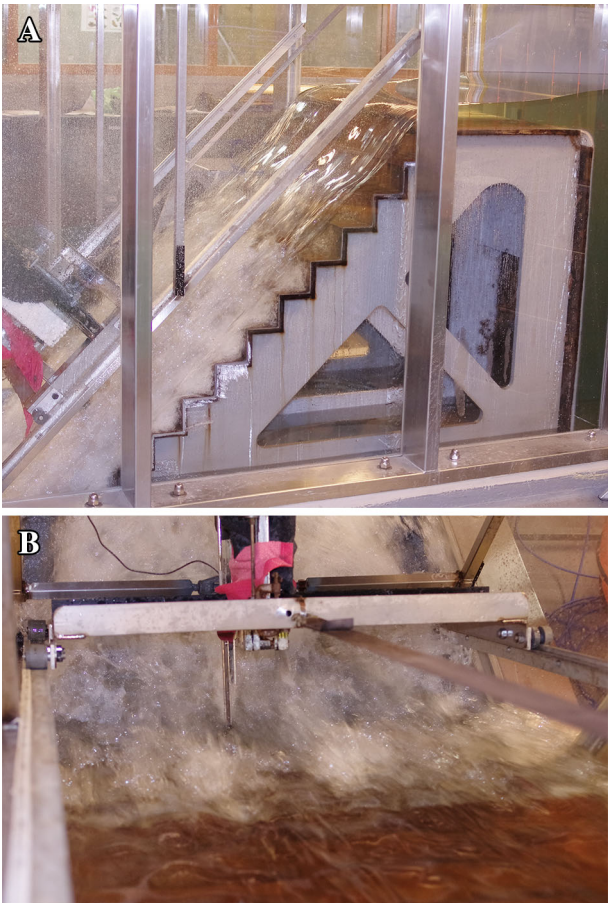

Fig. 5 Free-surface aeration in a large-size stepped spillway model ($\theta = 45°$, $h = 0.10$ m, $W = 0.985$ m). **a** General view—$d_c/h = 0.9$, $Re = 3.3 \times 10^5$, shutter speed: 1/80 s. **b** Details of free-surface structures next to the inception point of free-surface aeration, viewed from upstream—$d_c/h = 1.7$, $Re = 8.7 \times 10^5$, shutter speed: 1/80 s

an inner electrode of 0.25 mm diameter and sampled at 20 kHz for 45 s. Herein a nappe flow was observed for $d_c/h < 0.4$, where d_c is the critical flow depth: $d_c = (q^2/g)^{1/3}$, q is the discharge per unit width, g is the gravity acceleration and h is the vertical step height. A transition flow was observed for $0.4 < d_c/h < 0.9$. The present study is focused on the skimming flow regime observed for $d_c/h \geq 0.9$. The overflow skimmed over the pseudo-bottom formed by the step edges and the streamlines were approximately parallel to the pseudo-bottom, although the free-surface exhibited a wavy profile approximately in phase with the steps (Fig. 5). Downstream of the inception point of aeration, some complex air–water interactions were observed. The flow in step cavities exhibited a stable recirculation motion characterised by self-sustaining vortices, albeit irregular ejection of fluid from the cavity into the mainstream flow next to the upper vertical step face, and replacement of cavity fluid next to the step edge. Present observations indicated strong mainstream-cavity flow interactions as previously reported. Figure 5 presents two photographs of skimming flow conditions.

At each step edge downstream of the inception point, the void fraction data showed an inverted S-shape typically observed in self-aerated flows (Figs. 2, 4b and 6a). The air bubble concentration gradient $\partial C/\partial y$ was maximum in the mid-air–water column between $0.2 < y/d_c < 0.5$. At step edges, the data showed some self-similarity and a close agreement with analytical solutions (Fig. 4b), despite small scatter underlying void fraction and height measurements uncertainties. Typical void fraction distributions at step edges are presented in Fig. 6a.

The bubble count rate F, defined as half the number of air–water interfaces detected by the probe sensor per unit time, provides some information on the air–water flow fragmentation and is proportional to the specific interface area. Typical dimensionless bubble count rate $F \times d_c/V_c$ distributions are shown in Fig. 6a, where F is the bubble count rate defined as the number of bubbles detected per unit time and V_c is the critical flow velocity: $V_c = (g \times q)^{1/3}$. The data showed a distinct shape, with a maximum F_{max} at approximately $0.3 < y/d_c < 0.4$ corresponding to a void fraction between 0.4 and 0.5, as previously reported [5, 18, 25, 50]. The bubble count rate is linked to the flow fragmentation, characterised by characteristic length scales of a series of discrete water and air elements, denoted λ_w and λ_a respectively. A simplistic theoretical model may be developed by considering each air–water interface represented by two consecutive elements in different states [43]:

$$\frac{F}{F_{max}} = \frac{C \times (1 - C)}{\alpha \times \beta \times C_{F_{max}}^2} \tag{6}$$

where F_{max} is the maximum bubble count rate at a cross-section, C_{Fmax} is the corresponding void fraction, α is a parameter that accounts for differences between the average sizes of λ_w and λ_a, and β is a parameter allowing for variations of length scales:

$$\alpha = 1 + C \times \left(\frac{\lambda_w}{\lambda_a} - 1\right) \tag{7}$$

$$\beta = 1 - b \times (1 - 2 \times C)^4 \tag{8}$$

with b a coefficient that characterises the maximum variations of β with $(1-b) \leq \beta \leq 1$ [41, 43]. Note that the right hand side of Eq. (6) is proportional to the probability of occurrence of one pair of consecutive air–water elements. Equation (6) is compared to present data in Fig. 6b. A good agreement was found herein for $\lambda_w/\lambda_a = 2.2$ and $b = 0.4$.

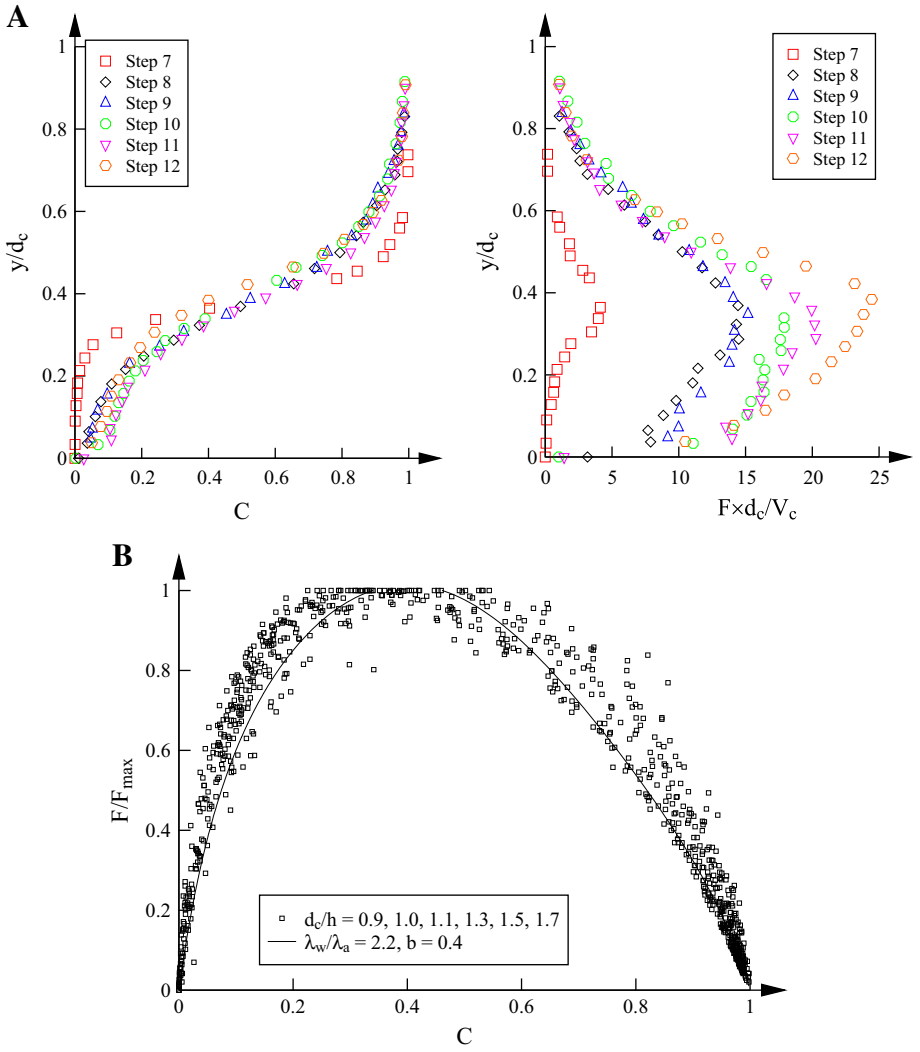

Fig. 6 Void fraction and bubble count rate distributions in skimming flow on a stepped chute ($\theta = 45°$, $h = 0.10$ m, $W = 0.985$ m). **a** Dimensionless void fraction and bubble count rate distributions for $d_c/h = 1.3$, $Re = 5.8 \times 10^5$ (free-surface aeration inception at step edge 7). **b** Relationship between void fraction and bubble count rate for $0.9 < d_c/h < 1.7$—comparison with Eq. (6)

A summary of observed values of λ_w/λ_a and b is provided in Table 2 for comparison. The present findings were in reasonable agreement with past studies.

The relationship between the root mean square of the instantaneous void fraction c_{rms} and the time-averaged void fraction C gives: $c_{rms} = C \times (1-C)$ [34]. That is, a parabolic relationship between time-averaged void fraction and void fraction root mean square and a maximum root mean square: $(c_{rms})_{max} = 0.25$. The bubble count rate is thus proportional to the root mean square of the instantaneous void fraction (Eq. 6) and the void fraction root mean square is maximum for $F = F_{max}$.

4 Discussion: air bubble diffusivity

4.1 Self-aeration in the rapidly-varied and gradually-varied flow regions

The apparent diffusivity of air bubbles D_a was deduced from the best fit of void fraction profiles, and the longitudinal distributions of dimensionless apparent diffusivities are presented in Fig. 7a. The rapidly-varied and gradually-varied flows regions, denoted RVF and GVF respectively, are separated by a red dotted line in Fig. 7. All data followed a self-similar distribution despite some scatter in the RVF region. The present data were best correlated by:

$$\frac{D_a}{\sqrt{g \times d_c^3}} = 0.027 \times \exp\left(-0.276 \times \frac{x - L_i}{L_{cav}}\right) \quad (R = 0.876) \tag{9}$$

where L_{cav} is the step cavity length: $L_{cav} = (h^2 + l^2)^{1/2}$, with h the vertical step height and l the horizontal step length The time varying diffusivity D_t may be solved by combining Eqs. (4) and (9):

$$\frac{D_t}{\sqrt{g \times d_c^3}} = 0.027 \times \left(1 - 0.276 \times \frac{x - L_i}{L_{cav}}\right) \times \exp\left(-0.276 \times \frac{x - L_i}{L_{cav}}\right) \tag{10}$$

Equation (10) is plotted in Fig. 7b. Basically the turbulent diffusivity decreases exponentially away from the inception point up to approximately $(x - L_i)/L_{cav} = 3.5$ and becoming negative further downstream. The turbulent diffusivity is linked to the rate of change of the mean void fraction C_{mean} (Appendix). Physically, in a one-dimensional model, a negative diffusivity indicates a negative rate of change of mean void fraction: i.e., some de-aeration and detrainment. This might happen when too much air is entrained

Table 2 Relationship between bubble count rate and void fraction: observations of λ_w/λ_a and b in stepped spillway flows

References	θ (°)	Flow regime (1)	λ_w/λ_a	b	Remarks
Present study	45.0	TRA, SK	2.2	0.4	$Re = 2.3 \times 10^5$ to 8.8×10^5
[49]	26.6	SK	2.4	0.55	Flat steps
			1.6	0.52	Gabion steps
[23]	26.6	TRA, SK	1–2.4	0.4–0.6	Flat steps
[43]	N/A	N/A	1.25 (lower nappe) 1.0 (upper nappe) 1.75 (spray and impact) 0.55–1.25 (downstream)	0.4 (lower nappe) 0.4 (upper nappe) 0.6 (spray and impact) 0.4 (downstream)	0.143 m drop
[25]	15.9	TRA II	1.75	0.41–0.71	$Re = 8 \times 10^4$ to 8.7×10^5
		SK	1.75	0.43–0.64	

TRA transition flow, *SK* skimming flow, *N/A* not relevant

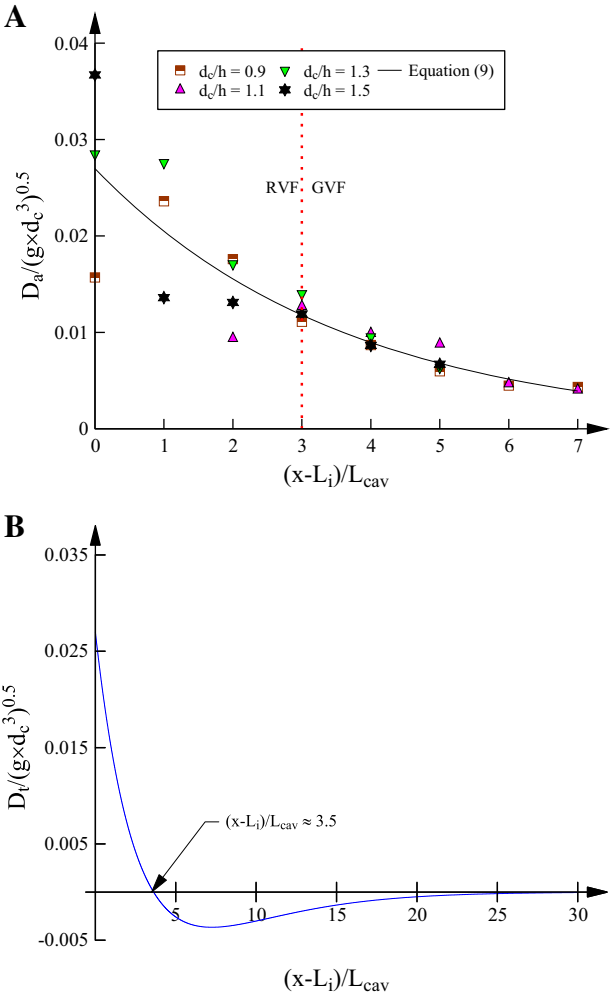

Fig. 7 Longitudinal distribution of dimensionless apparent and turbulent diffusivities in skimming flows. **a** Longitudinal distribution of apparent diffusivity D_a, based upon experimental data fitted using Eq. (3). **b** Longitudinal distribution of turbulent diffusivity D_t (Eq. 10)

initially and the flow must undergo a de-aeration process to attain equilibrium. Far downstream, the turbulent diffusivity would tend towards zero as the void fraction distribution approaches a pseudo-equilibrium. Yet Eqs. (3), (9) and (10) neglect the effect of buoyancy, which may be important in the uniform equilibrium region as illustrated in Eq. (5). At equilibrium, the turbulent diffusivity must be positive to balance out the effects of an upward bubble rise velocity. Herein the results suggest that the flow bulking stopped at approximately $(x - L_i)/L_{cav} = 3.5$ (Fig. 7b), and that the flow region upstream of this point may be classified as rapidly varied in terms of the mean void fraction.

Within its domain of application, Eq. (3) may be applied to predict the evolution of the depth averaged void fraction C_{mean} defined as:

$$C_{mean} = \frac{1}{Y_{90}} \times \int_{0}^{Y_{90}} C \times dy \quad (11)$$

Using the method of images, the lower limit of the integral may be replaced by $-Y_{90}$. Using Eq. (3) and after a change of variable, it yields:

$$C_{mean} = \frac{1.82 \times \sqrt{D_a \times t}}{Y_{50} + 1.82 \times \sqrt{D_a \times t}} \quad (12)$$

Note that $Y_{50} \approx d_i$ if the longitudinal acceleration due to gravity is small. The application of Eq. (12), using estimates of D_a and Y_{50} derived from measured void fraction data, showed some good agreement overall. The model reproduced accurately the mean void fraction at the inception point ($C_{mean} = 0.2$) while describing well the flow bulking in the rapidly-varied air–water flow region. Far downstream, the model estimates deviated slightly from measured data as the turbulent diffusivity decreased. If gravity effects are negligible, Eq. (12) may be used in conjunction with Eq. (9) assuming $Y_{50} = d_i$. This simplistic application is presented in Fig. 8, showing a reasonable estimate of the flow bulking downstream of the inception point where detailed diffusivity and depth data may not be available. It may be noted that the proposed air–water diffusion model imposes a theoretical maximum C_{mean} of 0.45 (for $t = \infty$) in a skimming flow. For comparison, an analytical model of Chanson and Toombes [18] imposed an upper limit of $C_{mean} = 0.60$ in a transition flow, suggesting that transition flows might be more effective in terms of re-aeration than skimming flows, albeit the presence of flow instabilities [19].

4.2 Interactions between air bubble diffusion and momentum transfer

For the gradually-varied and uniform equilibrium flow regions, the air bubble diffusivity may expressed in terms of the mean void fraction assuming a homogenous turbulence (Table 1), see Eq. (13a)—Chanson's model [13] and Eq. (13b)—Chanson and Toombe's model [18]:

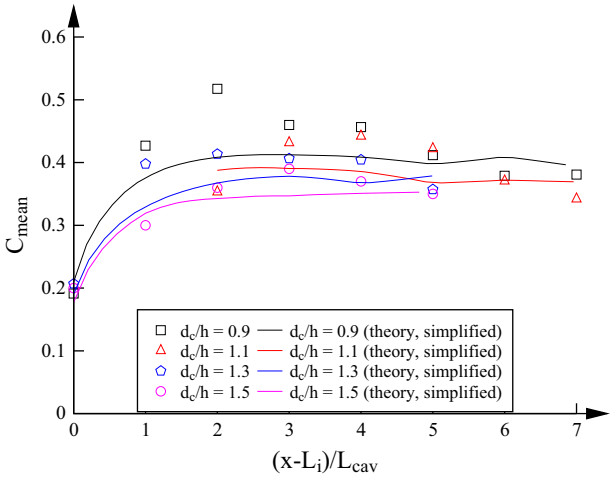

Fig. 8 Longitudinal distribution of mean void fraction C_{mean}: comparison between theory and data—calculations performed using Eq. (12) with simplified parameters

$$\frac{D_t}{Y_{90} \times \cos\theta \times (u_r)_o} = 0.7570 \times C_{mean}^{1.0104} \quad (13a)$$

$$\frac{D_t}{Y_{90} \times \cos\theta \times (u_r)_o} = \frac{-0.2767 \times \mathrm{Ln}(1.0434 - 1.312 \times C_{mean})}{1 - 2 \times \left(\frac{y}{Y_{90}} - \frac{1}{3}\right)^2} \quad (13b)$$

In Eq. (13b), D_t is not a constant across the air–water flow column and a depth averaged diffusivity may be calculated.

Adopting the mixing length theory and assuming a linear variation of shear stress across the fully-developed air–water column, the depth-averaged eddy viscosity ν_t in uniform equilibrium aerated flow may be approximated as:

$$\nu_t = \frac{\kappa}{6} \times V_* \times Y_{90} \quad (14)$$

where κ is the von Karman constant ($\kappa = 0.4$) and V_* is the shear velocity which may be estimated from the dimensionless shear stress f_e and flow velocity in the aerated flow region.

Present data are shown in Fig. 9 as functions of the Reynolds number Re defined in terms of the hydraulic diameter, and they are compared to past measurements in self-aerated flows. Figure 9 combines both laboratory and prototype data in smooth and stepped chutes, expanding the original analysis of Chanson [13]. Note that D_t is the depth-averaged

	Laboratory data	Prototype data
Smooth chutes	Straub and Anderson (1958) [UEF], Aivazyan (1986) [UEF]	Cain (1978) [GVF], Aivazyan (1986) [UEF]
Stepped chutes	Matos (1999) [UEF], Boes (2000) [UEF], Present study [GVF]	--

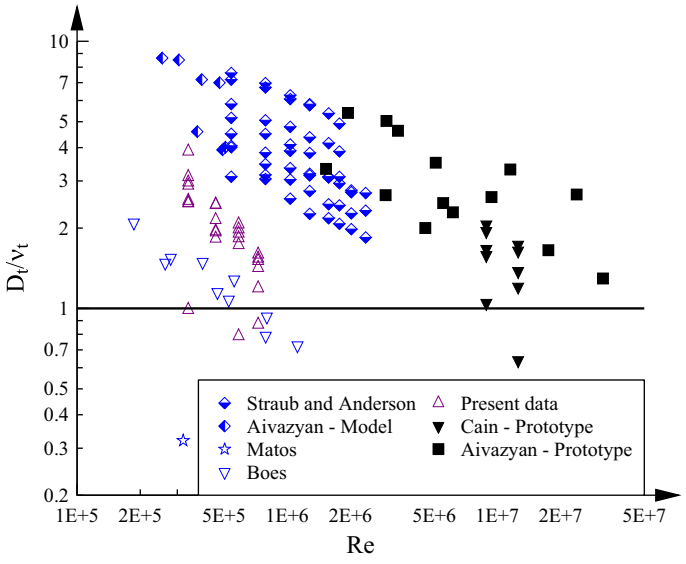

Fig. 9 Dimensionless depth-averaged diffusivity D_t/ν_T in gradually-varied and uniform equilibrium self-aerated flows—*UEF* uniform equilibrium flow, *GVF* gradually varied flow

diffusivity obtained by fitting the void fraction data. The results showed a ratio D_t/ν_t typically larger than unity, although with a decreasing trend with increasing Reynolds numbers (Fig. 9). For a given Reynolds number, some scatter was observed possibly when uniform equilibrium condition was not achieved: e.g., Cain's [7] prototype data in the gradually varied flow region, as well as with data sets including a wide range of invert slopes (e.g. [38]). Overall the observations expanded the earlier, limited finding of Chanson [13]. They indicate a clear trend of decreasing ratio of air bubble diffusivity to momentum exchange coefficient D_t/ν_t with increasing Reynolds number. Present results implied that a Froude similitude might not be sufficient to describe accurately the air bubble diffusion process in self-aerated smooth and stepped chute flows. The ratio D_t/ν_t is consistently larger in laboratory models than in prototype data, implying that physical modelling of self-aerated flows in laboratory over-represents the air bubble diffusion process in comparison to large prototype spillways.

It is acknowledged that a number of limitations in the present approach. In particular the expression for the momentum exchange coefficient ν_t (Eq. 14) assumed a linear variation in mixing length, which might not be appropriate in air–water chute flows, and in particularly in skimming flows on stepped spillways.

5 Conclusion

High-velocity chute flows consist typically of a clear-water flow region characterised by a turbulent developing boundary layer, followed by a self-aerated region in which large amounts of air are entrained. Immediately downstream of the inception point of free-surface aeration, the flow is rapidly-varied, and an analytical solution of the air diffusion equation is proposed. The result was successfully compared to new experimental data, predicting well the rapid self-aeration immediately downstream of the inception point. Both experimental observations and theoretical considerations show that the flow bulking stopped at approximately 3–4 step cavities downstream of the inception point on a stepped chute. Further downstream in the gradually-varied and uniform equilibrium flow regions, the void fraction distributions follow closely earlier solutions of the air diffusion equation, but for different boundary conditions. The air–water flow fragmentation may be characterised by the bubble count rate for a given void fraction. An unique relationship between bubble count rate and void fraction is observed in both smooth and stepped chute flows. The bubble count rate is proportional to the root mean square of the instantaneous void fraction and maximum values are observed for time-averaged void fractions between 0.4 and 0.5.

The solution of the air bubble diffusion equation implies turbulent diffusivities typically larger than, albeit close to, the momentum transfer coefficient. A re-analysis of both laboratory and prototype data is presented, covering nearly two orders of magnitude in terms of Reynolds numbers. The result indicates a marked decrease in ratio D_t/ν_t with increasing Reynolds number. This suggests that laboratory investigations of air bubble diffusion process in self-aerated flows might not be extrapolated to prototype applications without some form of scale effects. No scale effect will be observed at full scale only and the present finding reinforces a recommendation that: "*the future research into aerated flow hydraulics should focus on field measurements of high quality*" [17], in line with earlier argumentations [15, 29, 47].

Acknowledgments The authors acknowledge the technical of Jason Van Der Gevel and Stewart Matthews, School of Civil Engineering at the University of Queensland. Dr Hang Wang, School of Civil Engineering at the University of Queensland provided some helpful input. The authors further thank the reviewers and the SI editor Prof. Fabian Bombardelli for their helpful comments. The financial support of the Australian Research Council (Grant DP120100481) is acknowledged.

Appendix: Relationship between diffusivity and aeration

The sign of the diffusivity coefficient in a constant-property homogeneous turbulent flow governs the rate of change of the mean void fraction. Let us consider a two-dimensional self-aerated flow as illustrated in Fig. 3 and assume that the advective transport terms are small to negligible. The equation of conservation of mass for air may be expressed as [14]:

$$\frac{\partial}{\partial t}C = \mathrm{div}\left(D_t \times \overrightarrow{\mathrm{grad}C} - C \times \overrightarrow{u_r}\right) \tag{15}$$

where C is the time-averaged void fraction, D_t is the air bubble diffusivity and u_r is the bubble rise velocity. In the rapidly-varied flow region immediately downstream of the inception point, Eq. (15) may be reduced in first approximation into:

$$\frac{\partial C}{\partial t} = D_t \times \frac{\partial^2 C}{\partial y^2} \tag{16}$$

assuming that $\partial C/\partial x << \partial C/\partial y$ and neglecting buoyancy effects. The integration of Eq. (16) between 0 and Y_{90}, where Y_{90} is the characteristic elevation where $C = 0.9$, yields a relationship between the mean void fraction C_{mean} and the air bubble diffusivity:

$$\frac{d(C_{mean})}{dt} = \frac{D_t}{Y_{90}} \times \left(\left[\frac{\partial C}{\partial y}\right]_{y=Y_{90}} - \left[\frac{\partial C}{\partial y}\right]_{y=0}\right) \tag{17}$$

assuming a constant diffusivity throughout the air water column. In smooth chute flows and gradually varying skimming flows over stepped chute, the last term (in brackets) in Eq. (17) is positive, as illustrated in Figs. 2 and 6a. Thus the rate of change of mean void fraction has the same sign as the diffusivity. A positive diffusivity implies an increase in depth-averaged void fraction C_{mean} and some aeration. Conversely a negative diffusivity is associated with some de-aeration and detrainment (i.e. $\partial C_{mean}/\partial t < 0$) in a one-dimensional model.

Fig. 10 Schematic of fragmented flow downstream of a drop

For completeness, some fragmented flow may experience a negative term:

$$\left(\left[\frac{\partial C}{\partial y}\right]_{y=Y_{90}} - \left[\frac{\partial C}{\partial y}\right]_{y=0}\right) < 0 \quad (18)$$

Figure 10 illustrates an application of fragmented flow immediately downstream of a drop for which the data satisfy Eq. (18) [42, 44].

References

1. Aivazyan OM (1986) Stabilized aeration on chutes. *Gidrotekhnicheskoe Stroitel'stvo*, 12: 33–40 (in Russian). (Translated in Hydrotechnical construction, 1987, Plenum Publ., pp 713–722)
2. Anwar HO (1994) Self-aerated flows on chutes and spillways—discussion. J Hydraul Eng ASCE 120(6):778–779
3. Boes RM (2000) Zweiphasenstroömung und Energieumsetzung an Grosskaskaden (Two-phase flow and energy dissipation on cascades.) Ph.D. thesis, VAW-ETH, Zürich, Switzerland (in German). (also Mitteilungen der Versuchsanstalt fur Wasserbau, Hydrologie und Glaziologie, ETH-Zurich, Switzerland, No. 166)
4. Brattberg T, Chanson H, Toombes L (1998) Experimental investigations of free-surface aeration in the developing flow of two-dimensional water jets. J Fluids Eng Trans ASME 120(4):738–744
5. Bung DB (2009) Zur selbstbelüfteten Gerinnenströmung auf Kaskaden mit gemässigter Neigung (Self-aerated skimming flows on embankment stepped spillways.) Ph.D. thesis, University of Wuppertal, LuFG Wasserwirtschaft and Wasserbau, Germany, (in German)
6. Bung DB (2011) Developing flow in skimming flow regime on embankment stepped spillways. J Hydraul Res IAHR 49(5):639–648. doi:10.1080/00221686.2011.584372
7. Cain P (1978) Measurements within self-aerated flow on a large spillway. Ph.D. Thesis, Ref. 78-18, Dept. of Civil Engrg., Univ. of Canterbury, Christchurch, New Zealand
8. Cain P, Wood IR (1981) Measurements of self-aerated flow on a spillway. J Hydraul Div ASCE 107(HY11):1425–1444
9. Chamani MR (2000) Air inception in skimming flow regime over stepped spillways. In: Minor HE, Hager WH (eds) International workshop on hydraulics of stepped spillways. Balkema Publ., Zürich, pp 61–67
10. Chanson H (1989) Study of air entrainment and aeration devices. J Hydraul Res IAHR 27(3):301–319
11. Chanson H (1993) Self-aerated flows on chutes and spillways. J Hydraul Eng ASCE 119(2):220–243
12. Chanson H (1994) Hydraulics of skimming flows over stepped channels and spillways. J Hydraul Res IAHR 32(3):445–460
13. Chanson H (1995) Air bubble diffusion in supercritical open channel flow. In: Bilger RW (ed) Proceedings of the 12th Australasian fluid mechanics conference AFMC, Sydney, vol 2. pp 707–710
14. Chanson H (1997) Air bubble entrainment in free-surface turbulent shear flows. Academic Press, London
15. Chanson H (2009) Turbulent air-water flows in hydraulic structures: dynamic similarity and scale effects. Environ Fluid Mech 9(2):125–142. doi:10.1007/s10652-008-9078-3
16. Chanson H (2013) Interactions between a developing boundary layer and the free-surface on a stepped spillway: Hinze Dam spillway operation in January 2013. In: Proceedings of the 8th international conference on multiphase flow ICMF 2013, Jeju, Korea, 26–31 May, Gallery Session ICMF2013-005 (Video duration: 2:15). http://espace.library.uq.edu.au/view/UQ:301643. Accessed on 6 Aug 2015
17. Chanson H (2013) Hydraulics of aerated flows: qui pro quo? J Hydraul Res IAHR 51(3):223–243. doi:10.1080/00221686.2013.795917
18. Chanson H, Toombes L (2002) Air-water flows down stepped chutes: turbulence and flow structure observations. Int J Multiph Flow 27(11):1737–1761
19. Chanson H, Toombes L (2004) Hydraulics of stepped chutes: the transition flow. J Hydraul Res IAHR 42(1):43–54
20. Ehrenberger R (1926) Wasserbewegung in steilen Rinnen (Susstennen) mit besonderer Berucksichtigung der Selbstbelüftung (Flow of water in steep chutes with special reference to self-aeration.) Zeitschrift des Österreichischer Ingenieur und Architektverein, No. 15/16 and 17/18 (in German) (translated by Wilsey EF, U.S. Bureau of Reclamation)

21. Ervine DA, Falvey HT (1987) Behaviour of turbulent water jets in the atmosphere and in plunge pools. In: Proceedings of Institution of Civil Engineers, London, Part 2, vol 83. pp 295–314. Discussion: Part 2, Mar–June 1988, vol 85. pp 359–363
22. Falvey HT (1980) Air-water flow in hydraulic structures. USBR Engrg. Monograph, No. 41, Denver
23. Felder S (2013) Air-water flow properties on stepped spillways for embankment dams: aeration, energy dissipation and turbulence on uniform, non-uniform and pooled stepped chutes. Ph.D. thesis, School of Civil Engineering, The University of Queensland, Brisbane, Australia
24. Felder S, Chanson H (2013) Aeration, flow instabilities, and residual energy on pooled stepped spillways of embankment dams. J Irrig Drainage Eng ASCE 139(10):880–887. doi:10.1061/(ASCE)IR.1943-4774.0000627
25. Gonzalez CA (2005) An experimental study of free-surface aeration on embankment stepped chutes. Ph.D. thesis, Department of Civil Engineering, The University of Queensland, Brisbane, Australia
26. Hino M (1961) On the mechanism of self-aerated flow on steep slope channels. Applications of the statistical theory of turbulence. In: Proceedings of the 9th IAHR Congress, Dubrovnick, Yugoslavia, pp 123–132
27. Keller RJ, Rastogi AK (1977) Design chart for predicting critical point on spillways. J Hydraul Div ASCE 103(HY12):1417–1429
28. Killen JM (1968) The surface characteristics of self-aerated flow in steep channels. Ph.D. thesis, University of Minnesota, Minneapolis
29. Kobus H (1984) Scale effects in modelling hydraulic structures. In: Proceedings of international symposium on scale effects in modelling hydraulic structures, IAHR, Esslingen, Germany
30. Levi E (1965) Longitudinal streaking in liquid currents. J Hydraul Res 3(2):25–39
31. Matos J (1999) Emulsionamento de ar e dissipação de energia do escoamento em descarregadores em degraus (Air entrainment and energy dissipation in flow over stepped spillways.) Ph.D. thesis, IST, Lisbon, Portugal (in Portuguese)
32. Matos J (2000) Hydraulic design of stepped spillways over rcc dams. In: Minor HE, Hager WH (eds) International workshop on hydraulics of stepped spillways. Balkema Publ., Zürich. pp 187–194
33. Meireles I, Renna F, Matos J, Bombardelli F (2012) Skimming, nonaerated flow on stepped spillways over roller compacted concrete dams. J Hydraul Eng ASCE 138(10):870–877
34. Murai Y, Oishi Y, Takeda Y, Yamamoto F (2006) Turbulent shear stress profiles in a bubbly channel flow assessed by particle tracking velocimetry. Exp Fluids 41:343–352
35. Rao NSL, Gangadharaiah T (1971) Distribution characteristics of self-aerated flows. In: Rao RSL, Kobus H (eds) Characteristics of self-aerated free-surface flows. water and waste water/current research and practice, vol 10. Eric Schmidt Verlag, Berlin, pp 119–161
36. Rao NSL, Kobus HE (1971) Characteristics of self-aerated free-surface flows. In: Water and waste water/current research and practice, vol 10. Eric Schmidt Verlag, Berlin, Germany
37. Stewart WG (1913) The determination of the N in Kutter's formula for various canals, flumes and chutes on the boise project and vicinity. In: Report on 2nd annual conference on operating men, USBR, Boise, pp 8–23
38. Straub LG, Anderson AG (1958) Experiments on self-aerated flow in open channels. J Hydraul Div Proc ASCE 84(HY7):1890-1–1890-35
39. Takahashi M, Ohtsu I (2014) Analysis of nonuniform aerated skimming flows on stepped channels. Hydraulic structures and society—engineering challenges and extremes, The University of Queensland, Brisbane, Australia. In: Hubert C, Toombes L (eds) Proceedings of the 5th IAHR international symposium on hydraulic structures (ISHS2014), 25–27 June 2014, Brisbane, Australia, 9p. doi:10.14264/uql.2014.18
40. Thandaveswara BS, Rao NSL (1978) Developing zone characteristics in aerated flows. J Hydraul Div ASCE 104(HY3):385–396
41. Toombes L (2002) Experimental study of air-water flow properties on low-gradient stepped cascades. Ph.D. thesis, Dept of Civil Engineering, The University of Queensland, Brisbane, Australia
42. Toombes L, Chanson H (2007) Free-surface aeration and momentum exchange at a bottom outlet. J Hydraul Res IAHR 45(1):100–110. doi:10.1080/00221686.2007.9521748
43. Toombes L, Chanson H (2008) Interfacial aeration and bubble count rate distributions in a supercritical flow past a backward-facing step. Int J Multiph Flow 34(5):427–436. doi:10.1016/j.ijmultiphaseflow.2008.01.005
44. Toombes L, Chanson H (2008) Flow patterns in nappe flow regime down low gradient stepped chutes. J Hydraul Res 46(1):4–14. doi:10.1080/00221686.2008.9521838
45. Wood IR (1984) Air entrainment in high speed flows. In: Helmut K (ed) Proceedings of the international symposium on scale effects in modelling hydraulic structures, IAHR, Esslingen, Germany, paper 4.1, 7p

46. Wood IR (1985) Air water flows. In: Proceedings of the 21st IAHR congress, Melbourne, Australia, Keynote address. pp 18–29
47. Wood IR (1991) Air entrainment in free-surface flows. In: IAHR hydraulic structures design manual no. 4, hydraulic design considerations. Balkema Publ., Rotterdam, The Netherlands. 149p
48. Wood IR, Ackers P, Loveless J (1983) General method for critical point on spillways. J Hydraul Eng ASCE 109(2):308–312
49. Wüthrich D, Chanson H (2014) Hydraulics, air entrainment and energy dissipation on gabion stepped weir. J Hydraul Eng. 140(9):10. doi:10.1061/(ASCE)HY.1943-7900.0000919
50. Yasuda Y, Chanson H (2003) Micro- and macro-scopic study of two-phase flow on a stepped chute. In: Ganoulis J, Prinos P (eds) Proceedings of the 30th IAHR biennial congress, Thessaloniki, Greece, vol D. pp 695–702